



Department of Electronic & Telecommunication Engineering, University of
Moratuwa, Sri Lanka.

DESIGN AND IMPLEMENTATION OF A FULLY ANALOG LINE FOLLOWING ROBOT

Team Neural Nexus
Group Members:

Index No	Name
230487D	Lasan Perera
230051L	Isitha Dinujaya
230492M	Dulana Pitiwaduge
230502X	Deneth Priyadarshana

Supervisor: Mr. Tharusha Sihan

Submitted in partial fulfillment of the requirements for the module
EN 2091 Laboratory Practice and Projects

December 14, 2025

Abstract

Abstract A line follower robot is an analog autonomous system designed to track either a white line on a dark surface or a dark line on a light surface. In this project, our objective was to develop a robot capable of following a 3cm wide white line on a black background. While such robots are commonly implemented using microcontrollers such as the Atmega328P, ESP32 and STM32, this project required a fully analog approach. Therefore, all circuits were designed and constructed manually using operational amplifiers, resistors, potentiometers, and other analog components.

Abbreviations and Acronyms

CMRR Common-Mode Rejection Ratio

PWM Pulse Width Modulation

IR Infrared

LED Light Emitting Diode

PCB Printed Circuit Board

TWG Triangular Waveform Generator

Contents

1	Introduction	3
2	Methodology	4
2.1	Control System Architecture - Block Diagram	4
2.2	Electronic Circuit Design and Analytical Calculations	4
2.2.1	Component Selection	4
2.2.2	Infrared Sensor Array Design	5
2.2.3	Weighted Summation and Error Signal Generation (Scaling Adder)	5
2.2.4	PID Control System Implementation	7
2.2.5	Motor Control	7
2.2.6	Power Regulation and Distribution	13
3	PCB Design	15
3.1	PCB Layer Stackup	15
4	Mechanical Design and Enclosure	17
4.1	Enclosure and User Interface	17
4.2	Structural Support	17
4.3	Motor Mounting	17
5	Software Simulation and Hardware Testing	19
6	Contribution of Group Members	20
7	Conclusion	20

1 Introduction

The line following robot serves as a fundamental model for these systems, designed to autonomously navigate a specific path—typically a white line on a black surface—using optical feedback without relying on digital microcontrollers for sensor data processing and decision-making, this project explores the design and implementation of a fully analog line-following robot.

The primary objective of this project is to achieve stable autonomous navigation without the use of programmable logic or software algorithms. Instead, the control architecture is built entirely upon continuous-time signal processing principles. This approach shifts the complexity from code to hardware design, requiring precise component selection and circuit tuning to replicate the behaviors of a digital control loop.

The core functionality of the robot is achieved through three distinct analog subsystems, each driven by specific integrated circuits and sensors.

Optical Sensing (TCRT5000): The robot's interface with the physical environment is managed by an array of TCRT5000 reflective optical sensors. These components utilize an infrared emitter and a phototransistor to detect variations in surface reflectivity. As the robot deviates from the white line, the sensor array generates varying analog voltage levels proportional to the error in position, serving as the primary input for the control system.

Analog Signal Processing (LM324N): The "brain" of the robot is constructed using LM324N Quad Operational Amplifiers. Unlike a microcontroller that processes binary data, the LM324N operates on continuous voltage signals. In this design, these op-amps are configured to perform essential mathematical operations—such as signal amplification, weighted summation, and comparison.

Motor Actuation (L293D): To translate the low-power control signals from the op-amps into physical motion, the system utilizes the L293D motor driver. This high-current quadruple half-H driver acts as the power interface, allowing the delicate analog control circuitry to drive the DC gear motors. It enables bidirectional control, allowing the robot to accelerate, decelerate, and execute differential steering maneuvers to maintain its trajectory.

By integrating these components into a cohesive analog feedback loop, the robot demonstrates how sophisticated control behaviors such as proportional error correction—can be realized purely through hardware. The final product design is shown in Figure 5.

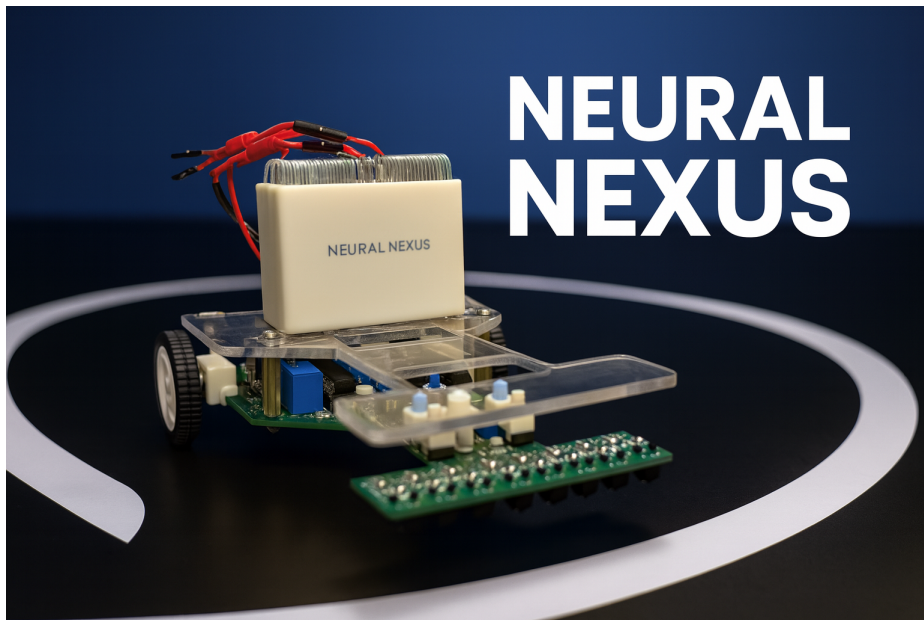


Figure 1: Final Product

2 Methodology

2.1 Control System Architecture - Block Diagram

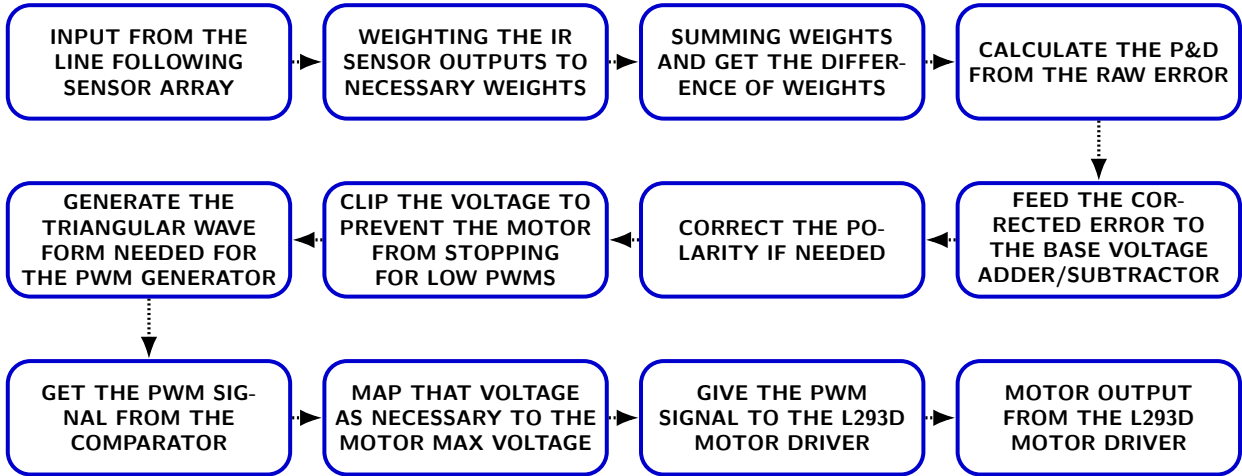


Figure 2: System Operational Flowchart

2.2 Electronic Circuit Design and Analytical Calculations

The following section presents the key electronic circuit blocks and their analytical considerations in our fully analog line follower robot:

- LM324MN op-amps for signal conditioning and control.
- IR sensor array converting surface reflectivity (white and black deviation) to electrical signals.
- Weighted summation circuits generate line error signals.
- Analog PD stage ensuring smooth trajectory correction to the robot.
- Triangular waveform generator supporting PWM creation.
- PWM module regulating motor speed.
- Motor driver circuits that deliver controlled power to the motors.
- Power regulation ensuring stable operation of all modules.

2.2.1 Component Selection

LM324MN Quad Operational Amplifier Analysis - The LM324MN is a widely used quad operational amplifier chosen for this project due to its **low cost, easy availability, high CMRR, and adequate slew rate(0.5V/ μ s)**. These characteristics make it suitable for signal conditioning and error detection in our fully analog line follower robot, ensuring reliable and fast response to sensor inputs.

L293D Motor Driver - The actuation of the robot is managed by the L293D, a quadruple high-current half-H driver integrated circuit. This component was selected to interface the low-power analog control signals with the high-current DC gear motors. The L293D is capable of providing continuous bidirectional drive currents of up to 600 mA per channel at operating voltages ranging from 4.5 V to 36 V. A critical feature of the 'D' variant is the inclusion of internal output clamp diodes. These diodes suppress the reverse inductive voltage spikes (back EMF) generated by the motors.

during switching, thereby protecting the sensitive operational amplifiers and signal conditioning circuitry from potential damage. In this design, the driver receives logic signals derived from the analog error correction stage and the PWM module to control the polarity and average voltage applied to the motors, enabling precise differential .

2.2.2 Infrared Sensor Array Design

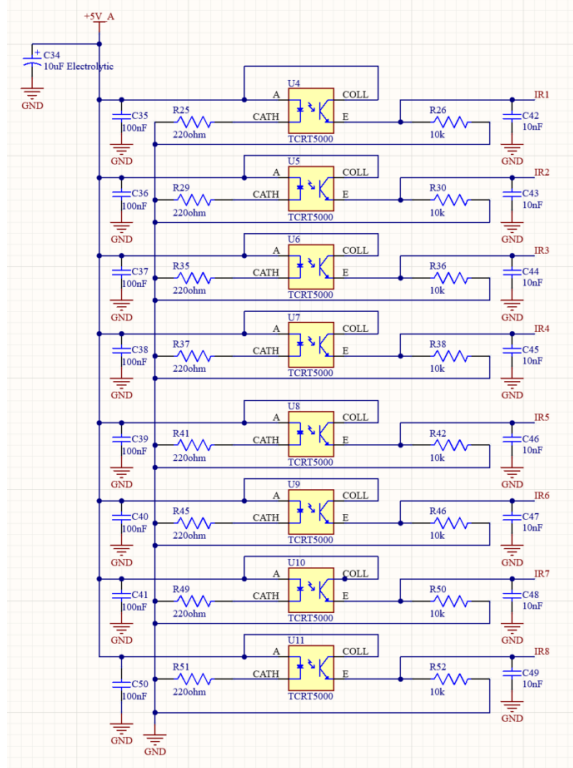


Figure 3: Sensor Array

Eight IR sensors, each with an IR LED and phototransistor (TCRT5000), detect the white line on the black surface. Their analog outputs are fed to comparators built using two LM324MN ICs, producing digital signals (0V/5V). The threshold is set at 3.3V using a variable potentiometer. We can change the threshold. Sensors are spaced 8mm apart, with the middle pair aligned to the line center for zero error. We used the analog reading from the sensor to the line sensing. We used the digital reading from the sensor to drive the led to tell the user whether the robot can read the line or not.

2.2.3 Weighted Summation and Error Signal Generation (Scaling Adder)

Error Signal Formation

In the analog line follower, the deviation from the line is represented by a continuous voltage signal generated through weighted summation of infrared (IR) sensor outputs. The sensors are arranged symmetrically on the right and left sides of the robot. The final error signal represents the difference between the weighted sum of the right-side IR sensors and the weighted sum of the left-side IR sensors.

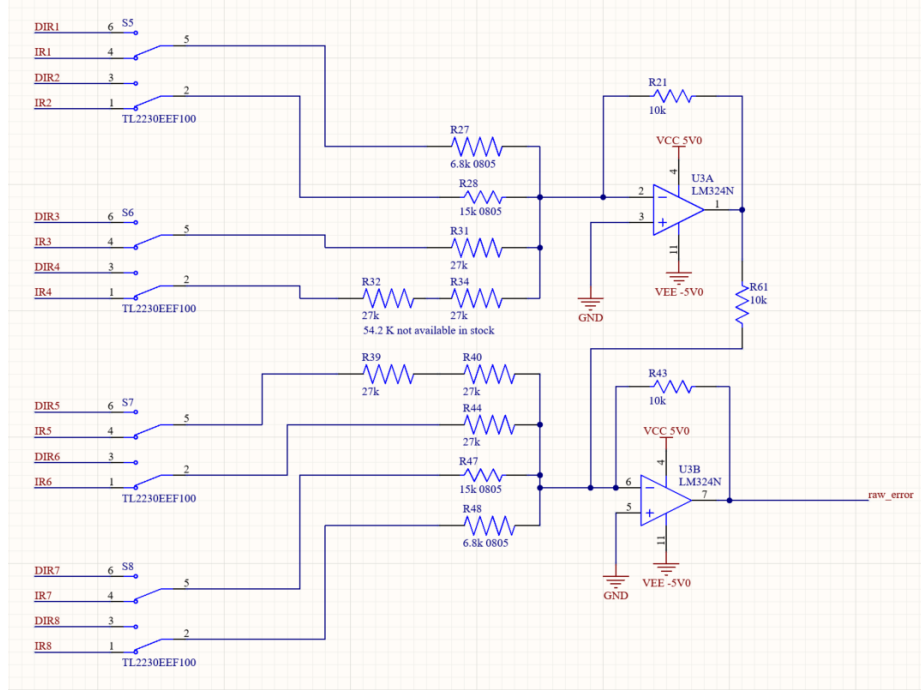


Figure 4: Scaling Adder

Role of Operational Amplifiers

The operational amplifier **U3A** is configured as an inverting summing amplifier and generates the negative weighted sum of the **right-side IR sensor voltages**. The operational amplifier **U3B** is also configured as an inverting summing amplifier and sums the **left-side IR sensor voltages** together with the output of U3A to form the final error signal.

Symbolic Derivation

The output of op-amp U3A, which sums the right-side IR sensors, is:

$$V_{U3A} = -R_{21} \left(\frac{V_{IR1}}{R_{27}} + \frac{V_{IR2}}{R_{28}} + \frac{V_{IR3}}{R_{31}} + \frac{V_{IR4}}{R_{32} + R_{34}} \right)$$

The output of op-amp U3B is obtained by summing the left-side IR sensor voltages together with the output of U3A:

$$V_{\text{raw_error}} = -R_{43} \left(\frac{V_{IR5}}{R_{39} + R_{40}} + \frac{V_{IR6}}{R_{44}} + \frac{V_{IR7}}{R_{47}} + \frac{V_{IR8}}{R_{48}} + \frac{V_{U3A}}{R_{21}} \right)$$

Substituting V_{U3A} and simplifying:

$$V_{\text{raw_error}} = R_{21} \underbrace{\left(\frac{V_{IR1}}{R_{27}} + \frac{V_{IR2}}{R_{28}} + \frac{V_{IR3}}{R_{31}} + \frac{V_{IR4}}{R_{32} + R_{34}} \right)}_{\text{Right IR sensor contribution}} - R_{43} \underbrace{\left(\frac{V_{IR5}}{R_{39} + R_{40}} + \frac{V_{IR6}}{R_{44}} + \frac{V_{IR7}}{R_{47}} + \frac{V_{IR8}}{R_{48}} \right)}_{\text{Left IR sensor contribution}}$$

Numerical Substitution

Using the circuit resistor values:

$$R_{21} = R_{43} = 10 \text{ k}\Omega$$

$$R_{27} = 6.8 \text{ k}\Omega, R_{28} = 15 \text{ k}\Omega, R_{31} = 27 \text{ k}\Omega, R_{32} + R_{34} = 54 \text{ k}\Omega$$

$$R_{39} + R_{40} = 54 \text{ k}\Omega, R_{44} = 27 \text{ k}\Omega, R_{47} = 15 \text{ k}\Omega, R_{48} = 6.8 \text{ k}\Omega$$

After substitution, the resistance values cancel, resulting in dimensionless weighting gains:

$$V_{\text{raw_error}} = (1.47 V_{IR1} + 0.67 V_{IR2} + 0.37 V_{IR3} + 0.19 V_{IR4}) - (0.19 V_{IR5} + 0.37 V_{IR6} + 0.67 V_{IR7} + 1.47 V_{IR8})$$

Interpretation

The final error signal is positive when the line is closer to the right side of the sensor array and negative when it is closer to the left. The cascaded summation using op-amps U3A and U3B ensures correct polarity and weighted contribution from each sensor, enabling smooth and stable analog line tracking.

2.2.4 PID Control System Implementation

The core function of the closed-loop control is executed by a proportional-derivative (PD) controller, implemented using operational amplifiers. The integral (I) term is deliberately omitted because the robot is a dynamic system in constant motion, and thus, correcting a static “steady-state error” defined here as the small, persistent positional error after initial stabilization is not required. The proportional gain (K_p) is adjusted by tuning the amplification of the K_p op-amp stage, providing a corrective torque proportional to the raw error. Simultaneously, the derivative gain (K_d) is controlled by varying the feedback resistance in the op-amp differentiator circuit, which dampens oscillations by reacting to the rate of change of the error signal. This PD approach ensures rapid and stable trajectory correction with reduced overshoot.

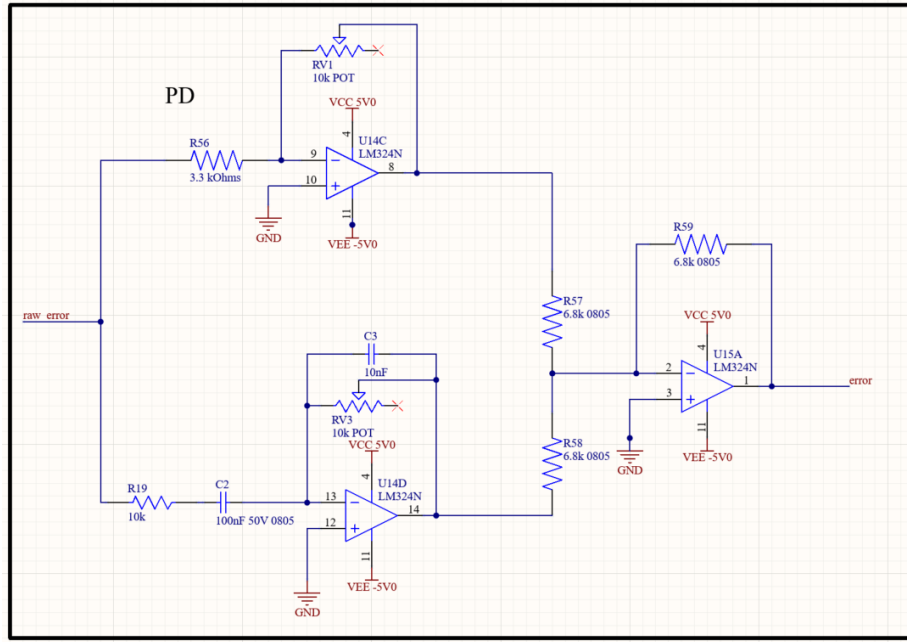


Figure 5: PD

2.2.5 Motor Control

TWG

In the analog line follower robot, pulse-width modulation (PWM) is used to control the motor speed smoothly based on the processed line sensor signal. For PWM generation, a stable triangular carrier waveform is required. This triangular wave is generated using a closed-loop analog oscillator formed

by a non-inverting Schmitt trigger and a ramp generator (integrator). The circuit operates only using analog components and does not require any external clock source.

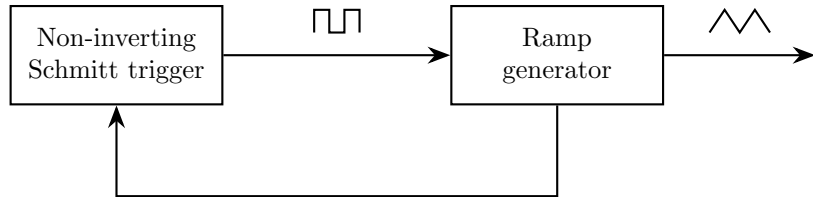


Figure 6: Block diagram of the triangular wave generator using a non-inverting Schmitt trigger and ramp generator

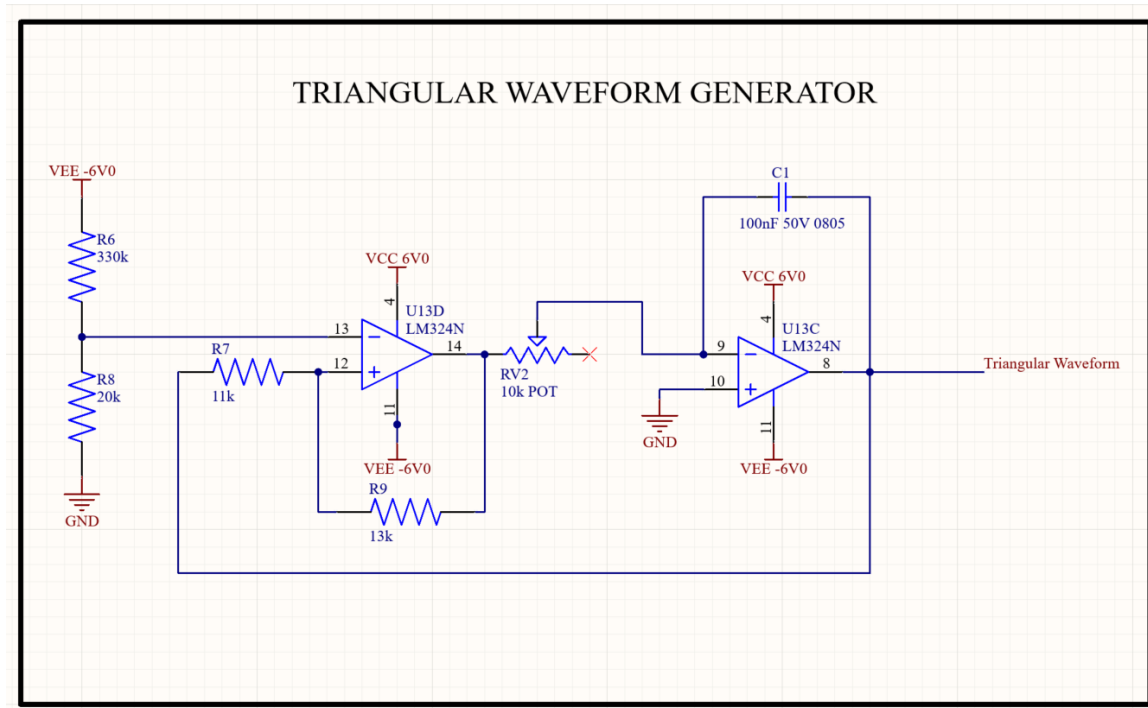


Figure 7: Circuit diagram of the triangular wave generator

Operating Principle

The non-inverting Schmitt trigger acts as a comparator with hysteresis and produces a square-wave output that switches between the LM324 operational amplifier saturation levels. Due to hysteresis, the Schmitt trigger has two well-defined switching thresholds.

The square-wave output is applied to the ramp generator, implemented using an op-amp integrator. Since the input voltage to the integrator remains constant during each state, the capacitor charges or discharges linearly, producing a ramp voltage.

The ramp generator output is fed back to the Schmitt trigger, forming a closed-loop system. When the ramp voltage reaches a switching threshold, the Schmitt trigger toggles and reverses the polarity applied to the integrator. This continuous action produces a stable triangular waveform.

Oscillation Frequency

The ramp generator is implemented as an op-amp integrator, where the slope of the ramp voltage is determined by the saturation voltage of the Schmitt trigger output and the integrator time constant.

The slope of the integrator output is given by:

$$\frac{dV}{dt} = \frac{V_{\text{sat}}}{R_{\text{V2}} C_1}$$

where R_{V2} is the effective resistance set by the potentiometer RV2 and C_1 is the integrator capacitor.

The ramp voltage swings between the upper and lower switching thresholds of the Schmitt trigger, denoted by V_{TH+} and V_{TH-} , respectively. The time required for the ramp voltage to transition between these thresholds is:

$$t = \frac{(V_{TH+} - V_{TH-}) R_{\text{V2}} C_1}{V_{\text{sat}}}$$

Since one complete oscillation consists of a rising ramp and a falling ramp, the total oscillation period is:

$$T = 2 \cdot \frac{(V_{TH+} - V_{TH-}) R_{\text{V2}} C_1}{V_{\text{sat}}}$$

Accordingly, the oscillation frequency of the triangular wave generator is:

$$f = \frac{V_{\text{sat}}}{2 R_{\text{V2}} C_1 (V_{TH+} - V_{TH-})}$$

Numerical Frequency Calculation

Since practical operational amplifiers do not exhibit equal positive and negative saturation voltages ($|V_{\text{sat}+}| \neq |V_{\text{sat}-}|$), a symmetric triangular waveform cannot be obtained when the Schmitt trigger reference voltage is tied to ground. To approximate symmetric operation, the reference voltage was shifted such that the resulting switching thresholds become nearly equal in magnitude. With this adjustment, the Schmitt trigger switching thresholds are approximately:

$$V_{TH+} \approx +4.5 \text{ V}, \quad V_{TH-} \approx -4.5 \text{ V}.$$

The need for this reference voltage shift and its implementation are discussed in a later subsection.

Thus, the total threshold swing is:

$$V_{TH+} - V_{TH-} = 9 \text{ V}$$

Using the design values:

$$C_1 = 100 \text{ nF}, \quad V_{\text{sat}} \approx 5 \text{ V}, \quad f \approx 600 \text{ Hz}$$

the required integrator resistance is obtained as:

$$R_{\text{V2}} = \frac{V_{\text{sat}}}{2fC_1(V_{TH+} - V_{TH-})}$$

$$R_{\text{V2}} = \frac{5}{2 \times 600 \times 100 \times 10^{-9} \times 9} \approx 4.6 \text{ k}\Omega$$

A 10 kΩ potentiometer (RV2) was therefore selected, with the nominal operating point set near the midpoint value of approximately 4.7 kΩ. This allows fine adjustment of the triangular wave frequency around 600 Hz to compensate for component tolerances and non-idealities.

Selection of the Integrator Capacitor

A capacitor value of 100 nF was selected to obtain a stable PWM carrier frequency while allowing sufficiently fast charging and discharging of the integrator capacitor. This avoids slew-rate limitations and ensures linear ramp generation. At the same time, the capacitance is large enough to reduce noise sensitivity and component tolerance effects.

Asymmetric Switching & Reference Voltage Shifting

Asymmetric switching in a non-inverting Schmitt trigger arises because practical operational amplifiers do not exhibit equal positive and negative saturation voltages:

$$V_{\text{sat}+} \neq |V_{\text{sat}-}|.$$

Since the switching thresholds are derived from these saturation levels through the positive feedback network, unequal saturation voltages result in inherently unequal upper and lower threshold voltages.

For the Schmitt trigger configuration used in this system, the switching thresholds are given by:

$$V_{\text{TH}+} = \left(1 + \frac{R_7}{R_9}\right) V_{\text{ref}} - V_{\text{sat}-} \frac{R_7}{R_9}$$

$$V_{\text{TH}-} = \left(1 + \frac{R_7}{R_9}\right) V_{\text{ref}} - V_{\text{sat}+} \frac{R_7}{R_9}.$$

Because $V_{\text{sat}+} \neq |V_{\text{sat}-}|$, the resulting switching thresholds are asymmetric when the reference voltage is tied to ground. To mitigate this effect and improve waveform symmetry, the reference voltage of the Schmitt trigger was shifted using a resistive voltage divider connected to the -6 V rail:

$$R_6 = 330\text{ k}\Omega, \quad R_8 = 20\text{ k}\Omega.$$

This divider sets the reference voltage to:

$$V_{\text{ref}} = -6 \times \frac{20}{330 + 20} \approx -0.34\text{ V}.$$

Shifting the reference voltage repositions the switching thresholds to be closer in magnitude, improving the symmetry and stability of the generated triangular waveform. However, complete symmetry cannot be achieved due to the inherent inequality of the op-amp saturation limits.

The triangular waveform generated by the TWG is compared with the control voltage derived from the line sensor processing circuit. This comparison determines the PWM duty cycle. As the control voltage varies with line position, the PWM duty cycle changes accordingly, enabling smooth and proportional motor speed control.

PWM Generation

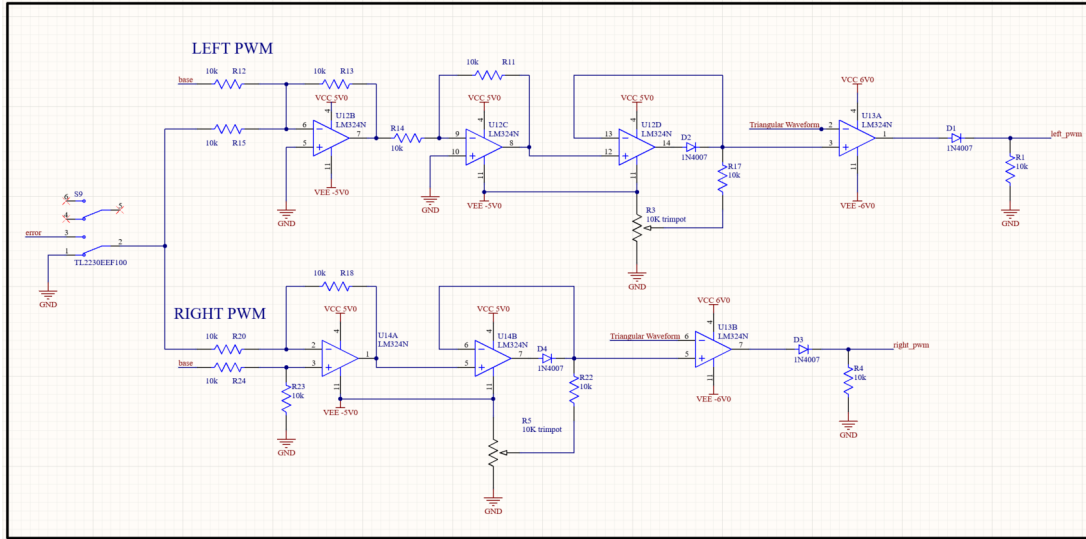
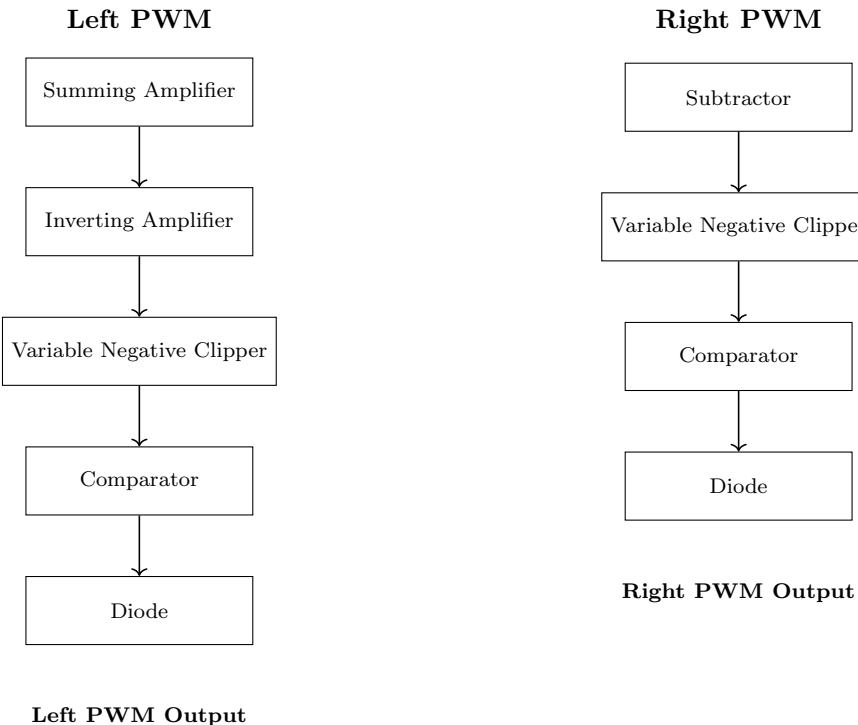


Figure 1: PWM generation circuit for left and right motor control

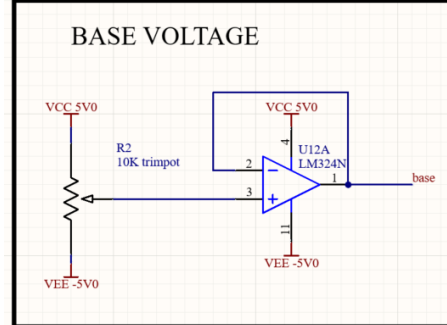
Block Diagrams



Left PWM Output

Base Voltage

The base voltage establishes the nominal motor drive level when the line-following error signal is zero. This voltage is generated using a potentiometer connected between the positive and negative supply rails. The adjustable node is buffered by an operational amplifier configured as a voltage follower. The buffering stage provides low output impedance, prevents loading effects, and ensures a stable reference voltage.



Base voltage generation and buffering circuit

When the base voltage is -5 V , the relevant base PWM duty cycle is 0%. When the base voltage is $+5\text{ V}$, the base PWM duty cycle reaches 100%. Intermediate base voltage values result in proportionally varying base duty cycles.

The buffered base voltage is distributed to both the left and right PWM generation paths, maintaining symmetry in the baseline motor speeds. By adjusting this voltage, the base motor speed can be tuned without affecting the differential steering behavior of the system.

PWM Generation Stages

The raw error signal is formed as the weighted difference between the right and left IR sensor outputs:

$$\text{raw_error} = (\text{scaled right IR signals}) - (\text{scaled left IR signals})$$

The raw error is then processed by the PD control system to generate the conditioned error signal used for motor control:

$$\text{error} = K_p \text{ raw_error} + K_d \frac{d}{dt}(\text{raw_error})$$

Summing and Inverting Amplifier (only for Left PWM)

In the left PWM channel, the base voltage and the processed error signal are combined using a summing amplifier. Due to the inverting configuration of the summing amplifier, the output of this stage is the negative of the desired sum, expressed as

$$V_{\text{sum}} = -(V_{\text{base}} + V_{\text{error}})$$

To restore the correct polarity, the output of the summing amplifier is passed through an inverting amplifier. This second inversion removes the negative sign introduced by the summing stage, resulting in the left motor control signal

$$V_{\text{control,L}} = V_{\text{base}} + V_{\text{error}}$$

This control signal represents the desired adjustment of the left motor speed relative to the nominal operating point. A positive error increases the control signal, while a negative error reduces it, enabling appropriate corrective steering action around the defined base motor speed.

Subtractor (only for Right PWM)

In the right PWM channel, a subtractor circuit is used to combine the base voltage and the processed error signal. This block generates the difference between the base voltage and the error signal, producing a control signal with complementary behavior to the left PWM channel. The output of the subtractor is given by

$$V_{\text{control,R}} = V_{\text{base}} - V_{\text{error}}$$

This control signal ensures that when the left motor speed is increased due to a positive error, the right motor speed is reduced by a corresponding amount. Such complementary action enables differential steering while maintaining a common base operating point.

Variable Negative Clipper

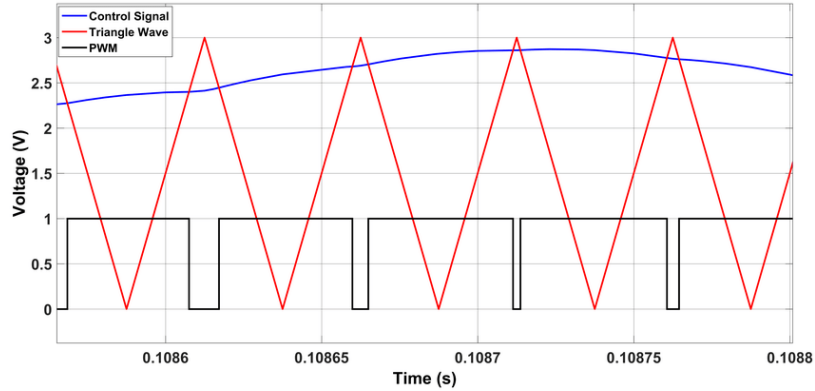
The control signals generated for both the left and right PWM channels are passed through a variable negative clipper. This block independently limits the minimum drive level applied to each wheel, thereby setting a lower bound on the motor speed.

The clipping threshold is adjustable, allowing fine tuning of steering sensitivity while limiting the maximum corrective action applied to the motors. This stage is primarily used to prevent either wheel from completely stopping during sharp turns, ensuring smooth motion and maintaining stability of the robot.

Comparator

Each clipped control signal is compared with a common high-frequency triangular waveform. The comparator switches its output state whenever the instantaneous value of the control signal exceeds the triangular carrier voltage.

This comparison converts the analog control signal into a pulse-width-modulated waveform, where the duty cycle is directly proportional to the magnitude of the control signal.



Example PWM generation by comparing a control signal with a triangular carrier waveform

Output Diode

A diode is placed at the output of each comparator to convert the bipolar comparator output into a unipolar PWM signal suitable for the motor driver input. The operational amplifier used as the comparator produces an output that swings between $+V_{sat}$ and $-V_{sat}$ (with $V_{sat} \approx 4.5$ V).

The diode blocks the negative saturation level and allows only the positive portion of the waveform to pass, resulting in a PWM signal that spans from 0 V to $+V_{sat}$. This unipolar PWM signal is compatible with the motor driver input requirements and ensures reliable and safe operation of the drive stage.

Motor IC

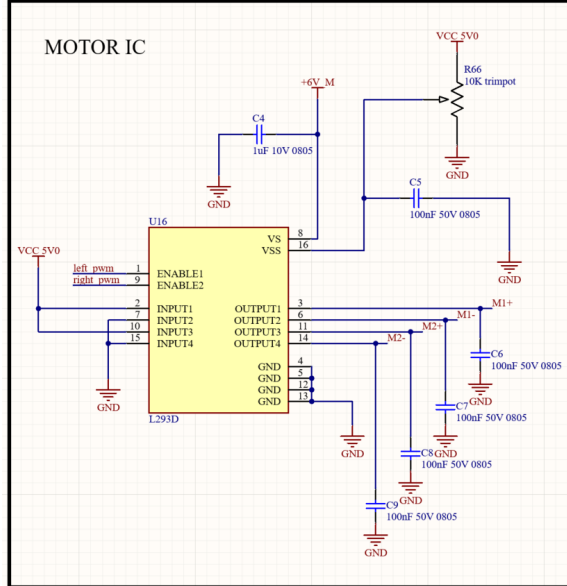


Figure 8: Motor Driver IC

2.2.6 Power Regulation and Distribution

The power management module, detailed in the circuit diagram, is crucial for converting the primary input voltage (V_{IN}) into multiple stable DC voltage rails required by the various components of the system.

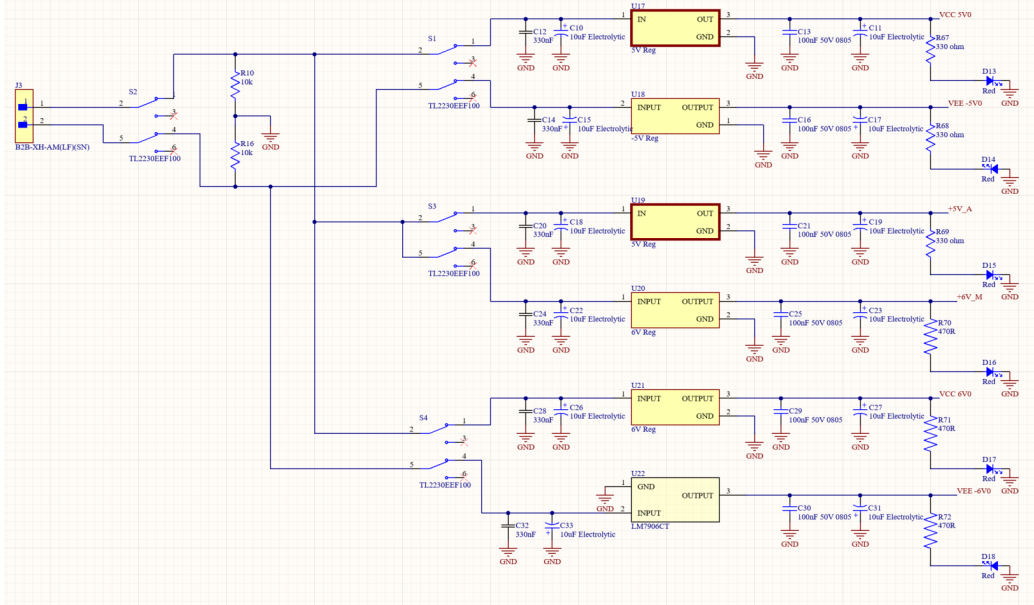


Figure 9: Power Distribution and Regulation Circuit Diagram

Key Functions and Rails - The module features several fixed-voltage regulators ($U_{17}-U_{21}$), which, along with the negative regulator U_{22} (LM7905CT), generate six regulated outputs. Input and output capacitors (e.g. $C_{10}-C_{31}$) are widely used for effective ripple reduction and noise filtering, ensuring clean power delivery.

The generated output rails are specifically tailored for system requirements:

- $+5V_A$: Dedicated supply for the **sensor array** circuitry.
- $+6V_M$: Dedicated power for the **motor** components.
- $\pm 5V$ ($+5V_{CC}, -5V_{EE}$): Bipolar supply primarily used for powering **operational amplifiers** and other analog components.
- $\pm 6V$ ($+6V_{CC}, -6V_{EE}$): For Motor Driver IC and powering **operational amplifiers**.

Power-on status is visually confirmed by the red LED indicators ($D_{13}-D_{19}$) on each output rail. Furthermore, the inclusion of switches (S_1-S_4 , TL2223EEF100) to enable power from the battery and then to selectively allow power into the voltage regulators for the purpose of debugging as well as to maintain the lifetime of the regulators.

3 PCB Design

3.1 PCB Layer Stackup

The circuit is implemented on a **four-layer Printed Circuit Board (PCB)**, a configuration specifically chosen to optimize signal integrity and power distribution. The sequential arrangement of the layers is as follows:

1. **Top Layer:** Dedicated to routing high-speed signal interconnects between surface-mount components.
2. **Layer 2 (Inner):** A solid **Ground Plane** (GND), providing a continuous, low-impedance return path for signals and acting as an electromagnetic interference (EMI) shield.
3. **Layer 3 (Inner):** A dedicated layer for the majority of the power rails (e.g., $+5V_{CC}$, $\pm 5V$), ensuring low impedance and stable voltage delivery across the board.
4. **Bottom Layer:** Used for routing less critical signals, and, crucially, carries the isolated **Motor Power Rail** ($+6V_M$). Placing the motor power here strategically segregates its potentially noisy path from sensitive signal and ground layers.

This stackup maximizes the benefits of closely coupled signal and ground layers, significantly enhancing signal quality and overall system reliability.

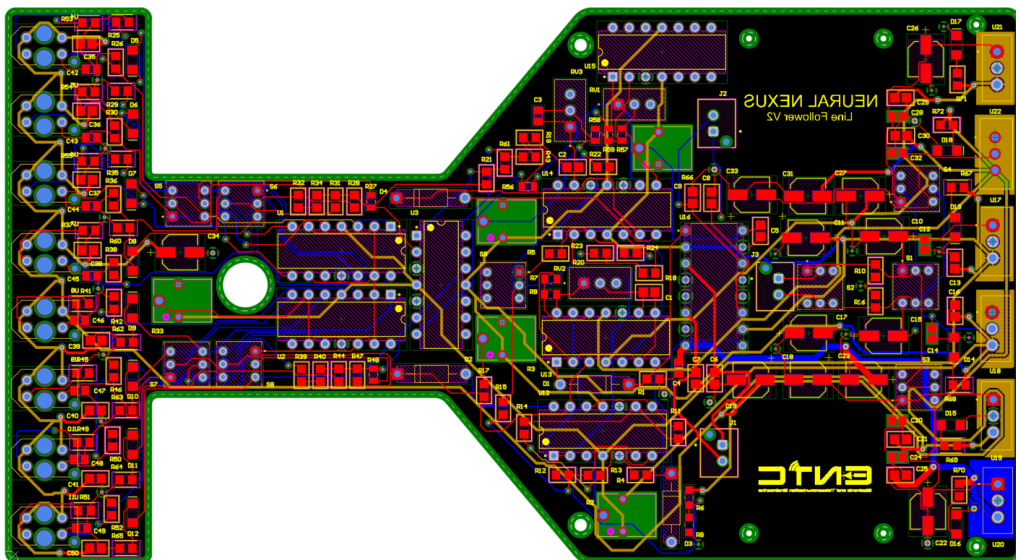


Figure 10: PCB 2D Layout

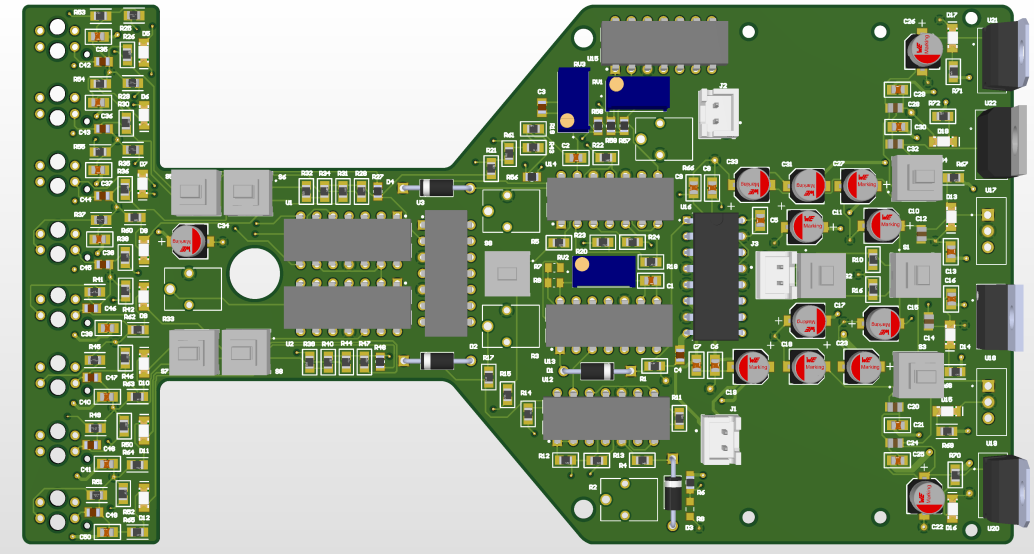


Figure 11: PCB 3D Top Layout

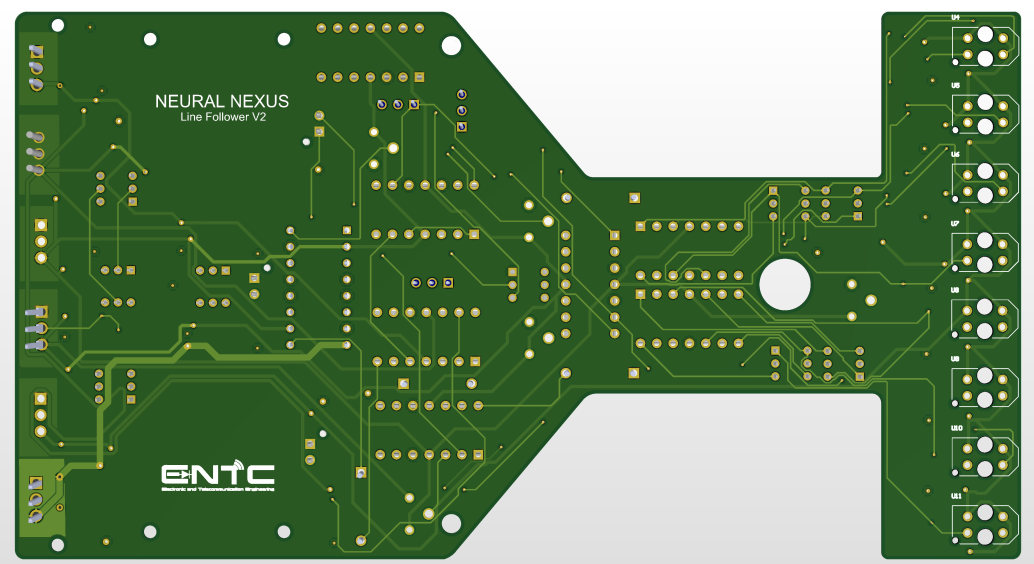


Figure 12: PCB 3D Bottom Layout

4 Mechanical Design and Enclosure

The mechanical assembly is designed for compactness, accessibility to components, and structural robustness. The system utilizes a four-legged chassis that supports a top-mounted Human-Machine Interface (HMI) sheet and custom motor integration.

4.1 Enclosure and User Interface

The enclosure is defined by a primary **top enclosing sheet** made from [Specify Material, e.g., 3mm acrylic]. This sheet acts as both a protective cover and the main control panel. Precision cutouts accommodate the user-accessible **potentiometers** for system tuning and **switches** for control activation. For convenient power management, the **battery holder** is externally mounted atop this sheet, enabling quick and tool-less battery replacement.

4.2 Structural Support

Structural stability is achieved using **four rigid support legs** (typically threaded standoffs) that are securely screwed directly to the main **Printed Circuit Board (PCB)**. This configuration elevates the PCB, protecting the bottom-layer components and ensuring a stable platform for the entire assembly.

4.3 Motor Mounting

The motor sub-system employs **custom-built motor brackets**. These brackets were specifically designed to meet the compact space constraints of the prototype, ensuring the motors are mounted with precise spatial alignment. This custom approach maintains the necessary mechanical precision required for the [briefly state motor function, e.g., system stability].

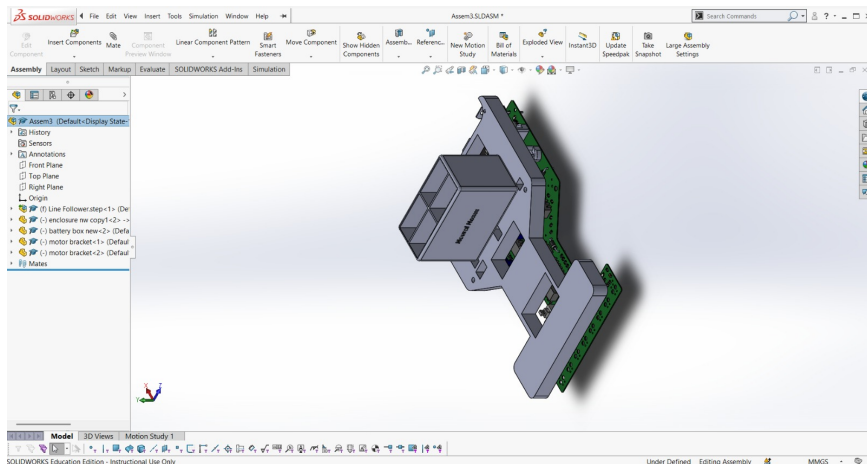


Figure 13: Robot Design

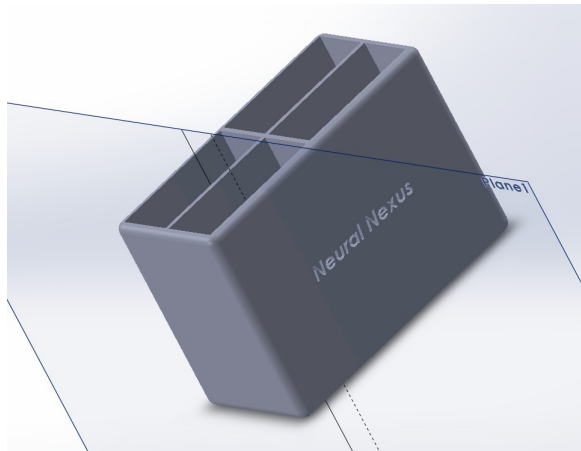


Figure 14: LIPO battery holder

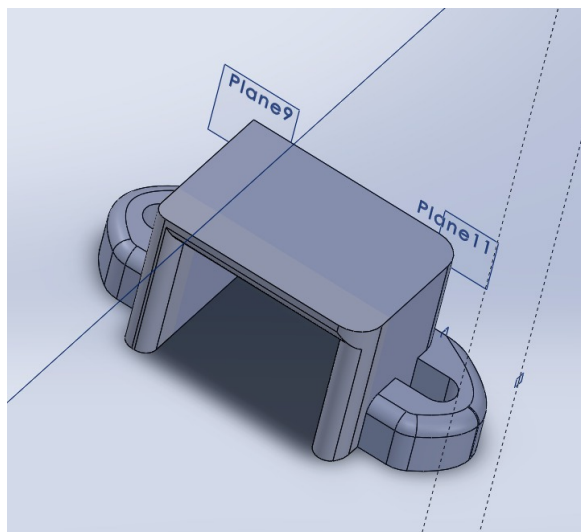


Figure 15: Custom Motor Bracket Design

5 Software Simulation and Hardware Testing

Simulations were run using the same circuits as the schematics above in LTspice and hardware testing were done on the breadboard with the help of the Oscilloscope and the Power Supply.

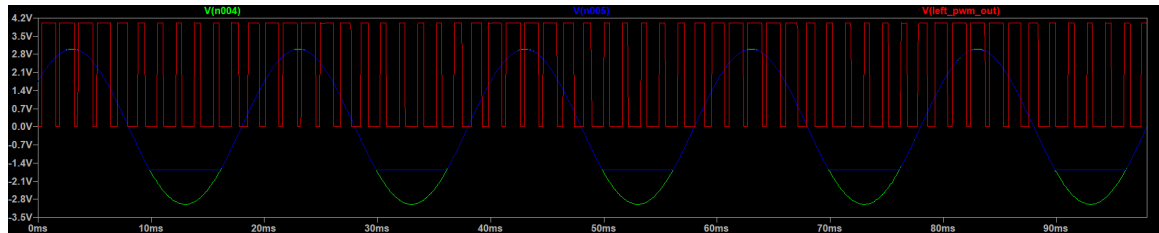


Figure 16: PWM generation, green shows base + error , blue shows base + error clipped

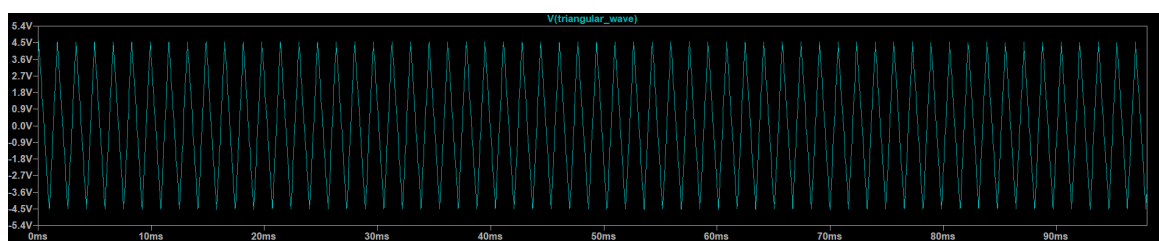


Figure 17: TWG simulation on LTspice

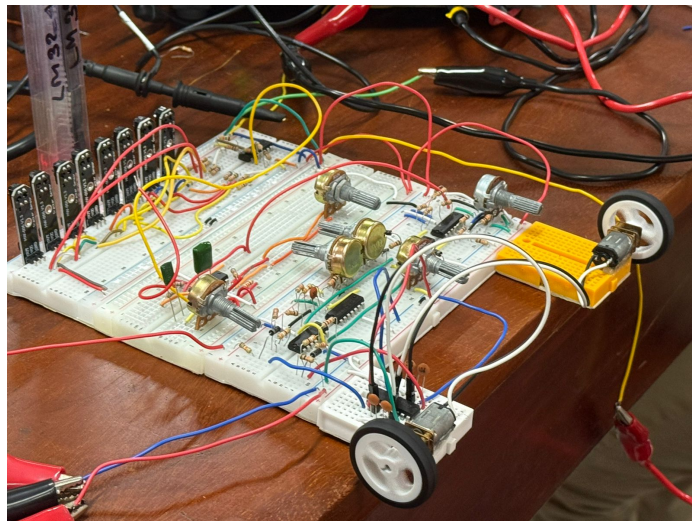


Figure 18: Breadboard Implementation

6 Contribution of Group Members

The successful completion of this project was the result of collaborative effort, with each team member taking responsibility for key areas under the supervision of a great supervisor.

- **Lasan Perera (230487D):** Led Soldering and Component Selection, the design and implementation of the Sensor Array, and contributed to the Power System hardware, role designation and logistics.
- **Isitha Dinujaya (230051L):** Responsible for the PD Control System development, overall Project Documentation, and the Enclosure Design.
- **Dulana Pitiwaduge (230492M):** Responsible for the PCB Design and Power System Design and acted as the lead for documentation and contributed for the TWG.
- **Deneth Priyadarshana (230502X):** Focused on Soldering, implementing the Motor Control Logic and TWG, and comprehensive system Debugging.

7 Conclusion

The design and implementation of the fully analog line-following robot successfully demonstrated that robust autonomous navigation can be achieved without the use of digital microcontrollers or software algorithms. By relying exclusively on continuous-time signal processing, the project met its primary objective of tracking a white line on a black surface using a custom-built analog control loop.

Key achievements of this project include:

- **Analog Signal Processing:** The successful implementation of a weighted summation network using LM324N operational amplifiers effectively translated physical sensor data into a continuous error voltage, proving that mathematical operations can be efficiently performed in hardware.
- **Control System Stability:** The integration of a Proportional-Derivative (PD) controller was critical in stabilizing the robot's movement. While the proportional term provided the necessary correction torque, the derivative term successfully damped oscillations, allowing for smooth tracking even at higher speeds.
- **Custom PWM Generation:** The development of a stable triangular waveform generator and comparator circuit replaced standard digital PWM timers, allowing for efficient motor speed control and power management via the L293D driver.
- **Noise Immunity:** The use of a four-layer PCB with dedicated ground and power planes significantly reduced signal interference, which is a common challenge in high-gain analog circuits.
- **Compact PCB design:** The use of a four-layer PCB with dedicated ground and power planes significantly reduced size of the PCB which would have not been possible with a two layer PCB. Form Factor plays a vital role in many applications.

This project highlighted the distinct trade-offs between analog and digital design. While analog systems offer zero-latency processing and eliminate the need for boot times or software debugging, they are more sensitive to component tolerances and environmental noise. Tuning the system required precise physical adjustments to potentiometers rather than simple code modifications. Ultimately, this project provided a comprehensive understanding of operational amplifier applications, feedback control theory, and power electronics, serving as a solid foundation for advanced electronic system design.

References

- [1] MIT OpenCourseWare, “6.071J Introduction to Electronics, Signals, and Measurement: Op Amps 3,” Spring 2006. [Online]. Available: https://ocw.mit.edu/courses/6-071j-introduction-to-electronics-signals-and-measurement-spring-2006/b713e408ddb359fd729360244e747aff_24_op_amps3.pdf
- [2] Jojo, “Triangular Waveform Using Schmitt Trigger,” *Circuits Today*, Sep. 22, 2009. [Online]. Available: <https://circuitstoday.com/triangular-waveform-using-schmitt-trigger>
- [3] National Instruments, “The PID Controller & Theory Explained,” Mar. 7, 2025. [Online]. Available: <https://www.ni.com/en/shop/labview/pid-theory-explained.html>